A Data

A.1 Seasat/Geosat

The observation data of Seasat and Geosat were obtained from the Radar Ice Altimetry project at Goddard Space Flight Center (GSFC, `https://icesat4.gsfc.nasa.gov/index.php`). We used the Ice Data Record (IDR) and for waveform retracking the respective Waveform Data Record (WDR). Orbit corrections for JGM-3 orbits were applied and measurements excluded if the noise level of the waveform was too high. For the GSFC data in our crossover comparison, we furthermore used the flags indicating when the leading edge definition failed or when problems occurred during retracking at all. Instead, for our retracked data, we calculated a signal to noise ratio (SNR) between the OCOG amplitude and the noise level and excluded shots with SNR < 3.

A.2 ERS-1/2

For ERS-1 and ERS-2 the SGRD data from the ESA REAPER (Reprocessing altimeter products for ERS) project (Brockley et al., 2017) was used. We excluded measurements where the flags in the data indicated a poor orbital or range measurement quality, where the tracking was lost, where waveforms are corrupted by high noise or other problems and where time jumps in the data occurred as reported in the pre-release calibration/validation ("RA L2 Validation Report", `https://earth.esa.int/documents/10174/1511090/REA-TR-VAL-L2-7001-3-1.pdf`).

Our accuracy and precision tests using crossover (see Sect. 2.2) showed, that the early mission phases of ERS-1, prior to 1992-04-14, contain many outliers which could not be identified by any flag or suspicious value. Thus, we decided to exclude all data of this period from our analysis.

A.3 Envisat

For Envisat we used the SGDR V2.1 data from ESA. Here we used the Ku-band measurements of its altimeter system RA-2 acquired during the entire operation period (May 2002 to April 2012). To remove potentially corrupted observations from the data, we used the *measurement confidence flags* to find recorded distances out of range and to identify problems in the onboard processing and data handling, in the ultra stable oscillator, the automatic gain control (AGC) or in the waveform samples. We furthermore used the *fault identifier*, the *tracker range validity flag* and the *ICE1 retracking validity flag* to exclude invalid measurements.

A.4 ICESat

For ICESat the Release 34 GLA12 dataset from the National Snow and Ice Data Center (NSIDC) was used (exactly as in Schröder et al., 2017). We apply the saturation correction (Fricker et al., 2005) to the elevations and exclude all data where flags indicate off-nadir operation, orbit maneuvers or any other factors degrading the orbit accuracy. We also remove data where the attitude flag indicates any problem with star trackers, gyro or the laser reference sensor. In order to exclude data affected by forward scattering in clouds or drifting snow (e.g. Siegfried et al., 2011), we reject all returns with a gain value exceeding 200, with a reflectivity below 10%, with a misfit between the received waveform and the Gaussian model exceeding 0.03 V or where more than one waveform is detected (Bamber et al., 2009). We applied the inter-campaign biases determined by Schröder et al. (2017).

A.5 CryoSat-2

As in Schröder et al. (2017) we used the CryoSat-2 L2I product from ESA in the recent processing version Baseline C. For LRM we excluded all data where the *height error flag* indicates problems in the overall height determination. This flag is specific for each retracking method, hence, it also informs about problems of the respective retracker. For SARIn mode, we used the retracking scheme described in Helm et al. (2014) using a 40%-TFMRA retracker. The Star Tracker mispointing angles corrected for the aberration of light were applied prior the phase processing. This correction is explained in (Scagliola et al., 2017) and the data set provided by ESA. "Bad waveforms" are screened using a waveform filter (Helm et al., 2014) while for LRM, we again apply our SNR filter (SNR $<$ 3).

B Reprocessing

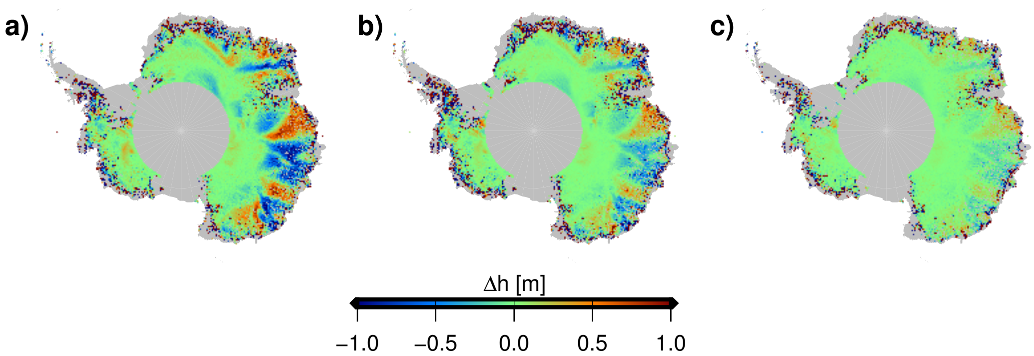

Figure S1: Bias between ascending and descending orbits for 3 different processing versions of the Envisat data: **a)** ESA version with ICE-2 retracker, **b)** ESA version with ICE-1 retracker and **c)** our reprocessed data with 10%-threshold retracker.

In order to assess the performance of our reprocessed data, we compare near time ascending-descending crossover differences (Fig. S2) as described in Sect. 2.2. As standard product to compare with, we use the widely used functional fit retracker version (GSFC Version 4 β-retracker for Seasat and Geosat, the ICE-2 retracker for ERS and Envisat and the default CFI retracker for CryoSat-2) and the respective slope correction from the data center (direct slope correction for GSFC, relocated by mean surface slope for ESA).

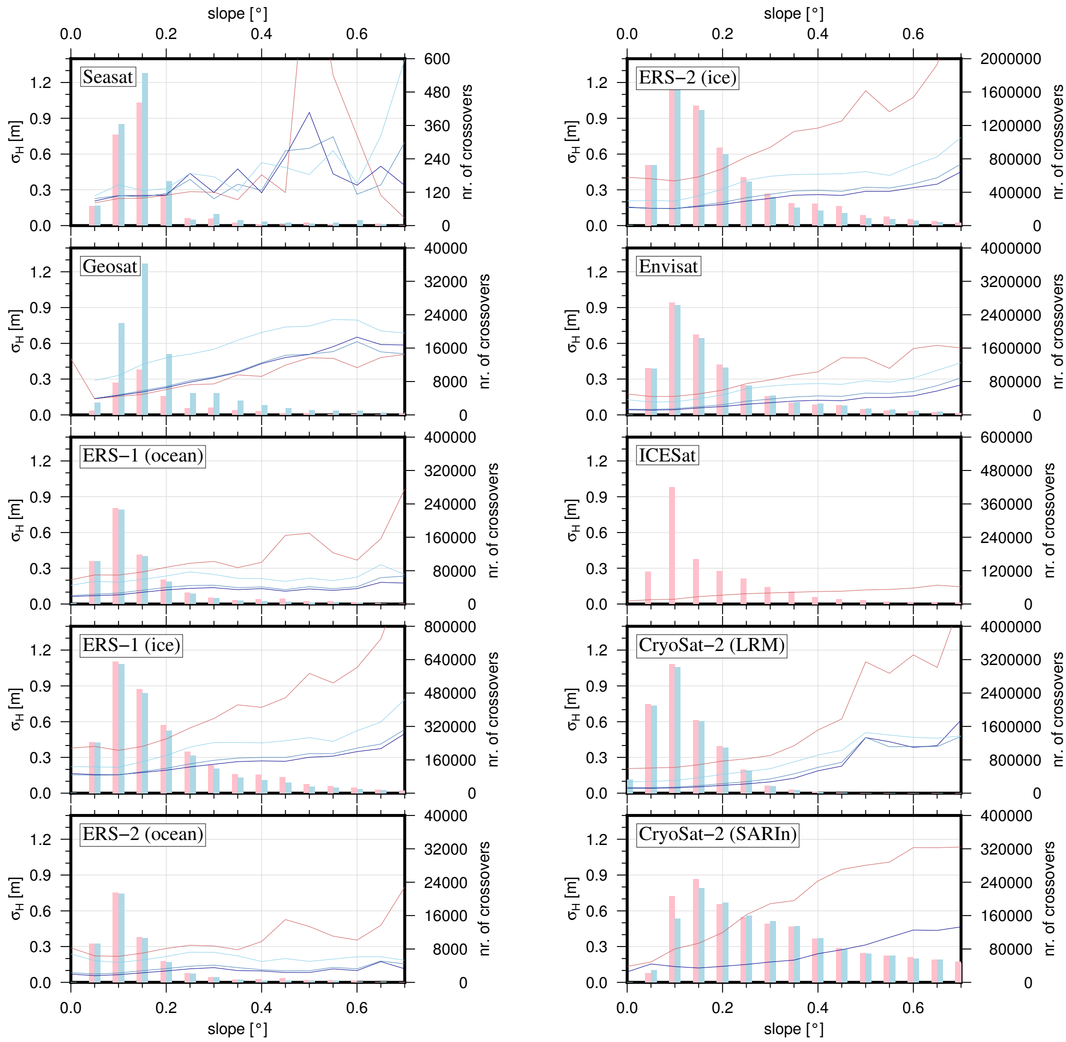

Figure S2: Measurement precision from near time (<31 days) crossovers, binned against slope ($\sigma_H = |\Delta H|/\sqrt{2}$). Red denotes the data provided by the respective data centers (see description above), light, medium and dark blue stands for our reprocessed data with 50%-, 20%- and 10%-threshold retracker, respectively and relocated using our refined approach. For CryoSat-2 SARIn, dark blue denotes the 40%-TFMRA (Helm et al., 2014). The bars in the background indicate the number of crossovers for the standard product (red) and our 10% (blue) data.

C Mission offsets

As described in Sect. 3.2 simultaneous epochs have been used to merge the time series of overlapping missions. If the dataset has no overlap with the reference mission (Envisat), the offsets need to be summed up. Due to the better spatial and temporal coverage of ERS's ice mode, the ocean mode biases have been determined w.r.t. ice mode and added to the specific ice mode offset. For ERS-1 in ocean mode ($ERS1_O$), this is calculated as

$$\Delta h_{ERS1_O-ENVI} = \Delta h_{ERS1_O-ERS1_I} + \Delta h_{ERS1_I-ERS2_I} + \Delta h_{ERS2_I-ENVI} \tag{1}$$

Figure S3 shows the sums of the respective offsets, which have been applied to our reprocessed data.

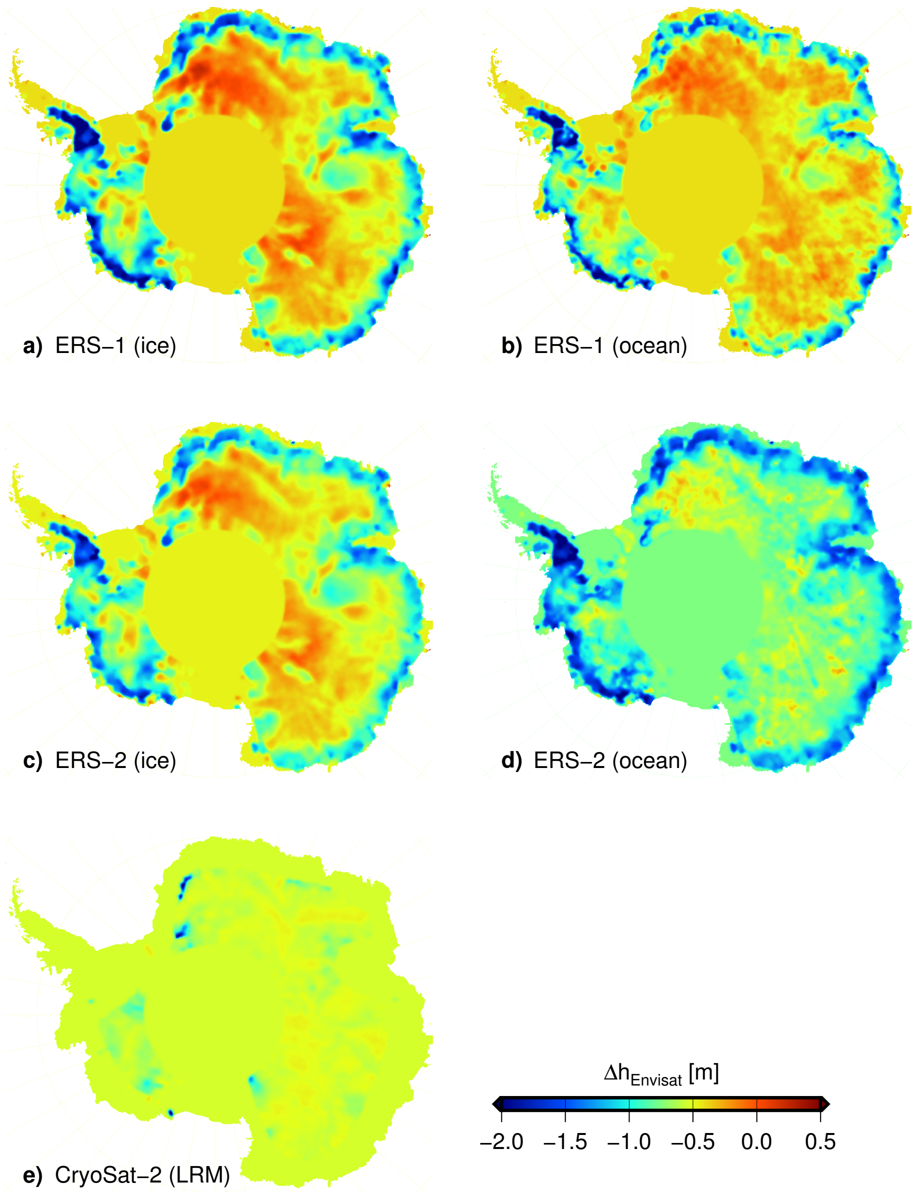

Figure S3: Offsets applied for calibrating the pulse limited radar altimetry data with our reference mission Envisat. In unobserved regions (as the polar gap or the SARIn zone of CryoSat-2) the grids are filled with the mean value.

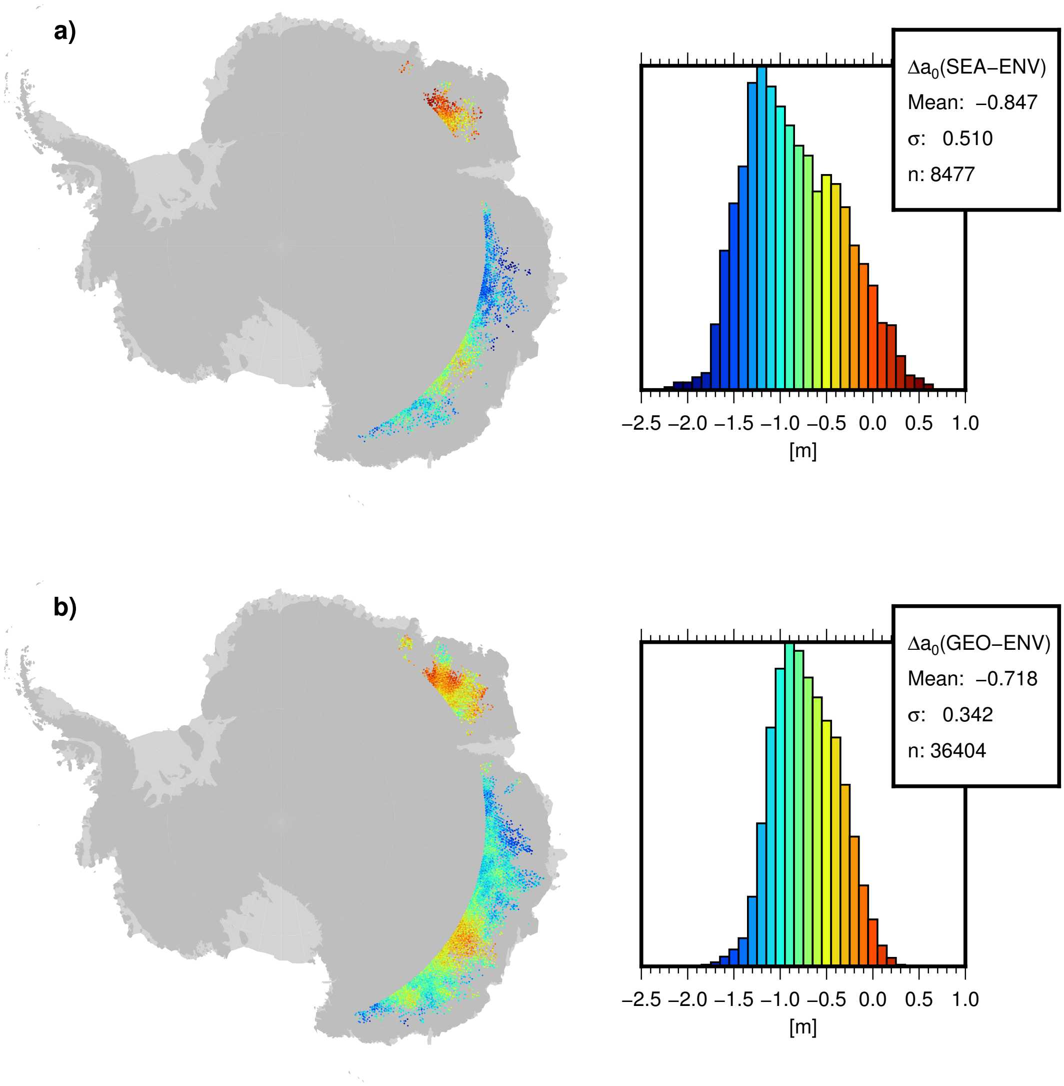

Figure S4: Offsets between **a** Seasat and Envisat and **b** Geosat and Envisat from cells which satisfy our criterion of a stable linear SEC rate.

D Linear rates

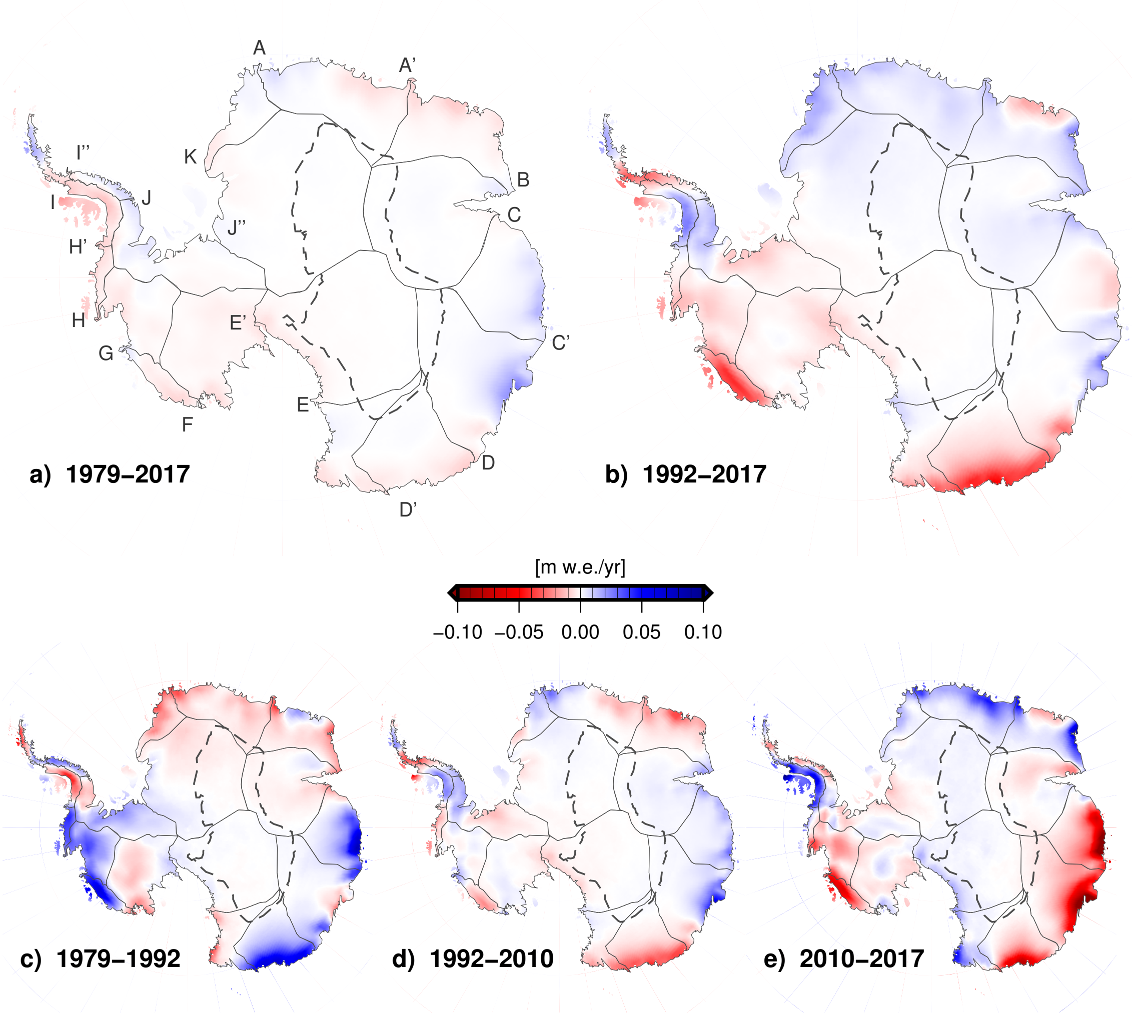

Figure S5: Linear rates fitted to the time series of ERA-Interim precipitation anomalies over different time intervals similar to Fig. 6. The solid lines mark the drainage basin outlines, the dashed line shows the outline of the low precipitation zone. **a)** Trends for the full time interval since 1979, **b)** trends since 1992 and **c-e)** trends for different sub-intervals.

E Basin time series

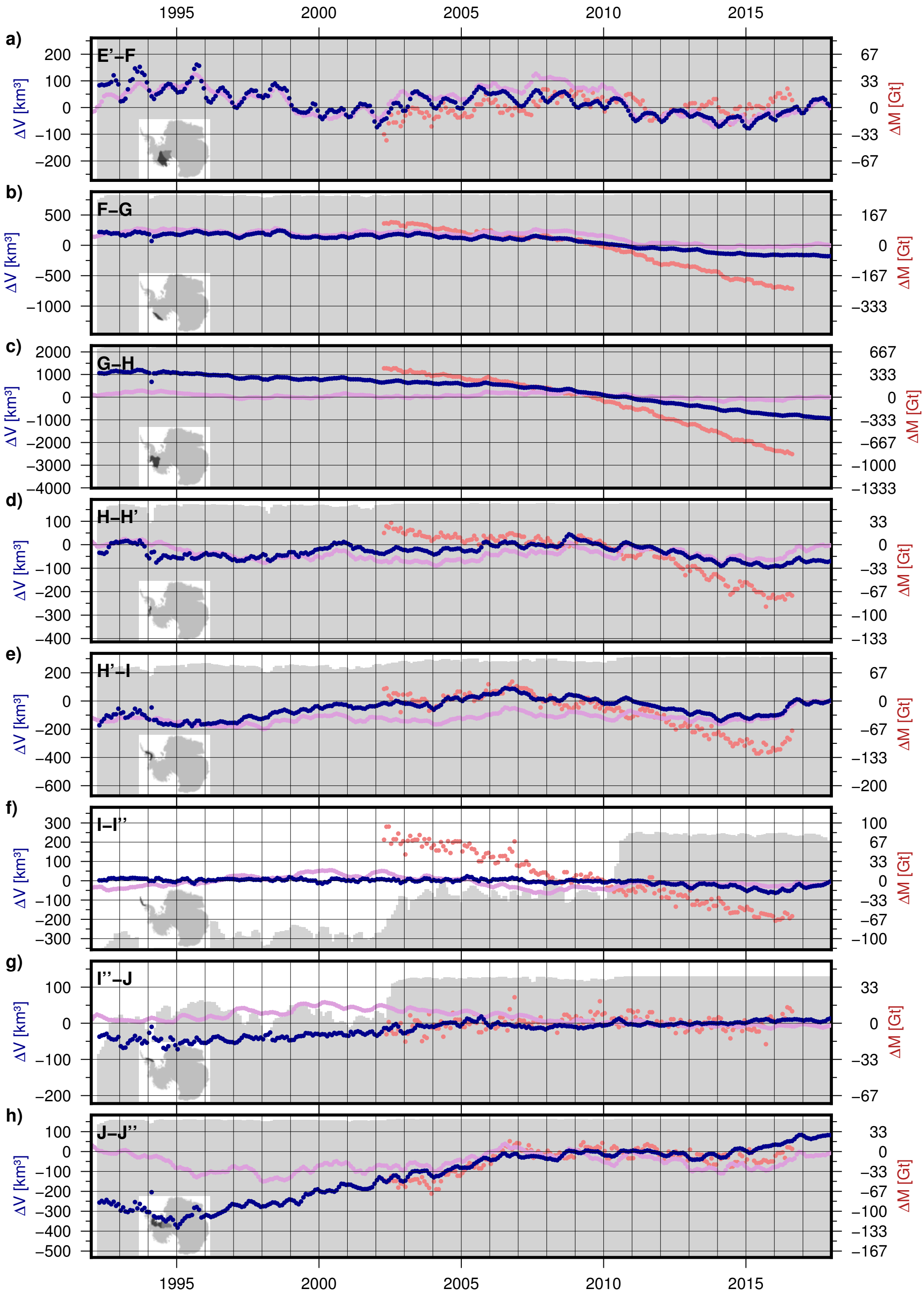

Figure S6: Volume change of the drainage basins in West Antarctica north of 81.5°S from our combined altimetric time series (blue). The respective time series of mass change from GRACE (red) and precipitation anomaly (pink) refer to the scale at the right. The gray color in the background displays the fraction of the area covered by observations (up to the top means 100%).

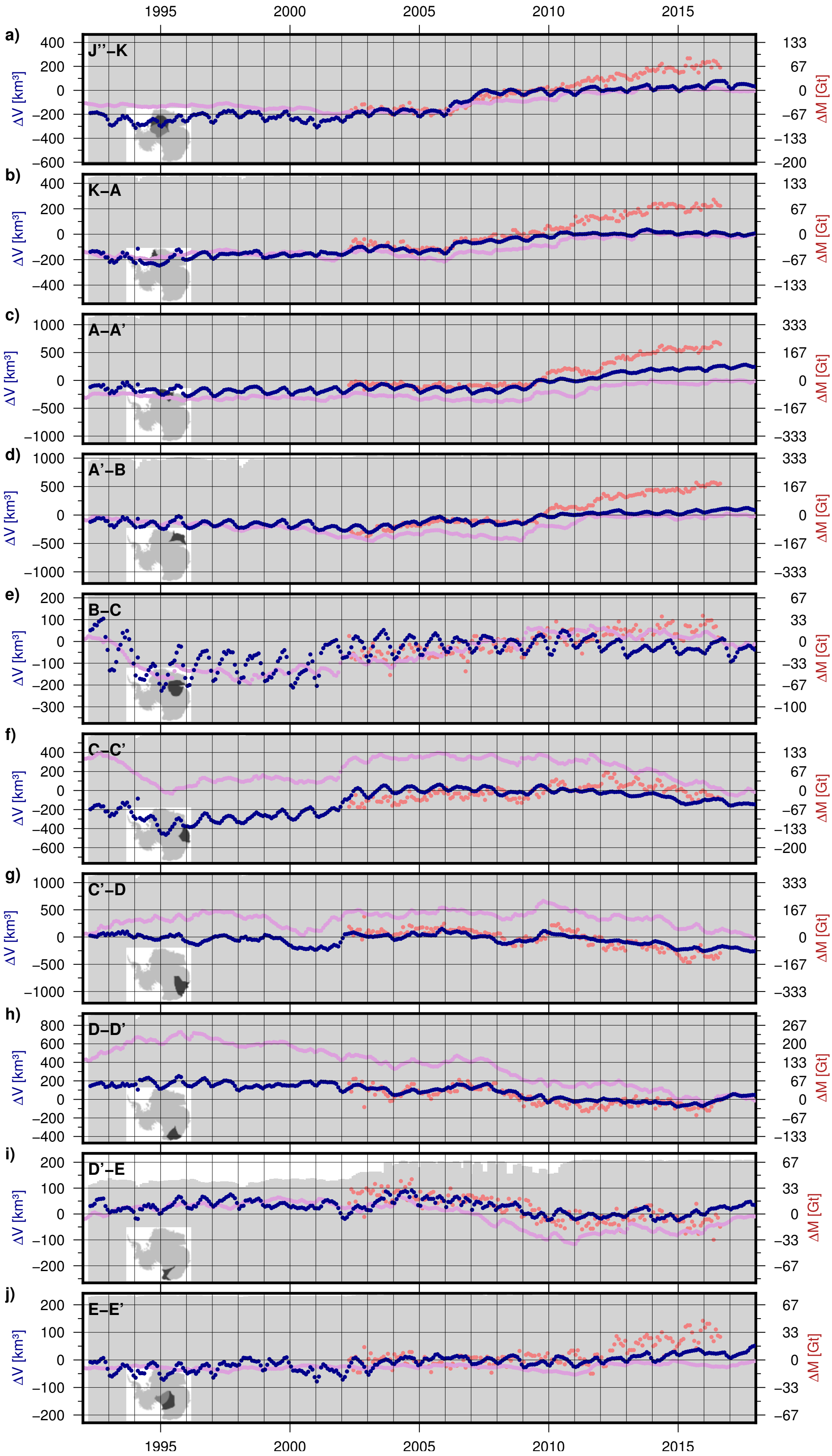

Figure S7: Volume change as in Fig S6, but for East Antarctic basins.

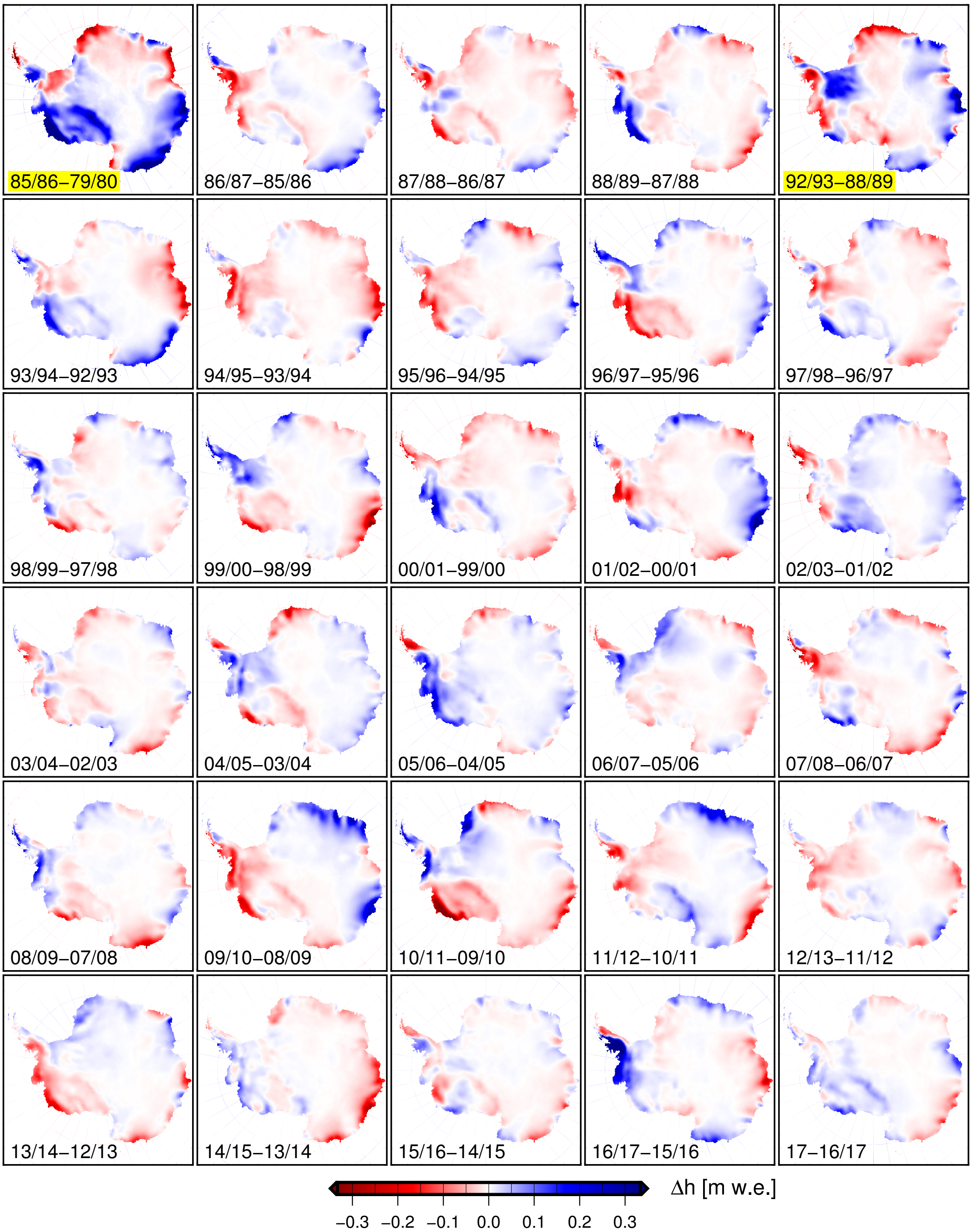

Figure S8: Elevation difference between the yearly mean water equivalent precipitation anomaly (July to June of next year) of consecutive years. Marked in yellow are differences spanning more than one year due to altimetry data gaps. Note that the first epoch differs slightly from the first altimetry epoch due to data availability.

References

Bamber, J., Gomez-Dans, J., and Griggs, J. (2009). A new 1 km digital elevation model of the Antarctic derived from combined satellite radar and laser data – Part 1: Data and methods. *The Cryosphere*, 3:101–111.

Brockley, D., Baker, S., Femenias, P., Martinez, B., Massmann, F.-H., Otten, M., Paul, F., Picard, B., Prandi, P., Roca, M., Rudenko, S., Scharroo, R., and Visser, P. (2017). REAPER: Reprocessing 12 Years of ERS-1 and ERS-2 Altimeters and Microwave Radiometer Data. *IEEE Trans. Geosci. Remote Sens.*, 55(10):5506–5514.

Fricker, H., Borsa, A., Minster, B., Carabajal, C., Quinn, K., and Bills, B. (2005). Assessment of ICESat performance at the salar de Uyuni, Bolivia. *Geophys. Res. Lett.*, 32:L21S06.

Helm, V., Humbert, A., and Miller, H. (2014). Elevation and elevation change of Greenland and Antarctica derived from CryoSat-2. *The Cryosphere*, 8(4):1539–1559.

Scagliola, M., Fornari, M., Bouffard, J., and Parrinello, T. (2017). The CryoSat interferometer: End-to-end calibration and achievable performance. *Adv. Space Res.*

Schröder, L., Richter, A., Fedorov, D., Eberlein, L., Brovkov, E., Popov, S., Knöfel, C., Horwath, M., Dietrich, R., Matveev, A., Scheinert, M., and Lukin, V. (2017). Validation of satellite altimetry by kinematic GNSS in central East Antarctica. *The Cryosphere*, 11(3):1111–1130.

Siegfried, M., Hawley, R., and Burkhart, J. (2011). High-Resolution Ground-Based GPS Measurements Show Intercampaign Bias in ICESat Elevation Data Near Summit, Greenland. *Geoscience and Remote Sensing, IEEE Transactions on*, 49(9):3393–3400.